Chinese Chemical Letters 35 (2024) 109727

Contents lists available at ScienceDirect

Chinese Chemical Letters

journal homepage: www.elsevier.com/locate/cclet

Recent progress of ultrasound-responsive titanium dioxide sonosensitizers in cancer treatment

Haijing Cui[a,b,1], Weihao Zhu[a,b,1], Chuning Yue[a,b], Ming Yang[b], Wenzhi Ren[a,b,c,*], Aiguo Wu[b,c,*]

[a] Cixi Biomedical Research Institute, Wenzhou Medical University, Ningbo 315300, China
[b] Ningbo Key Laboratory of Biomedical Imaging Probe Materials and Technology, Zhejiang International Cooperation Base of Biomedical Materials Technology and Application, Chinese Academy of Sciences (CAS) Key Laboratory of Magnetic Materials and Devices, Ningbo Cixi Institute of Biomedical Engineering, Zhejiang Engineering Research Center for Biomedical Materials, Ningbo Institute of Materials Technology and Engineering, Chinese Academy of Sciences, Ningbo 315201, China
[c] Advanced Energy Science and Technology Guangdong Laboratory, Huizhou 516000, China

ARTICLE INFO

Article history:
Received 27 December 2023
Revised 23 February 2024
Accepted 25 February 2024
Available online 7 March 2024

Keywords:
Titanium dioxide
Sonodynamic therapy
Reactive oxygen species
Cavitation effects
Combined therapy

ABSTRACT

Sonodynamic therapy (SDT) exhibits promising clinical applications in cancer treatment owing to its advantages, including ultrasonic cavitation effect, mechanical effect, and deep tissue penetration. Titanium dioxide (TiO_2) nanomaterials, recognized as excellent sonosensitizers, have been extensively studied in cancer SDT. This review first outlines the mechanism of TiO_2-based SDT, then systematically discusses the regulation of TiO_2 sonosensitivity, covering aspects such as morphology, particle size, element doping, defect engineering, heterojunction structure, and interactions with the tumor microenvironment. Furthermore, the review generalizes ultrasound-responsive TiO_2-based therapeutic modalities for tumor treatment, including SDT, SDT combined with chemotherapy, chemodynamic therapy, photothermal therapy, immunotherapy, and treatment visualization. Finally, the review navigates the ongoing challenges and prospects in TiO_2-based cancer SDT.

1. Introduction

According to the latest statistical report, although the cancer mortality rate in 2020 was 33% lower than that of 30 years ago due to the continuous development of treatment methods, global cancer death cases still reached 9.96 million [1]. Therefore, developing more efficient and safe new strategies for cancer treatment is of significant importance for improving patients' quality of life and increasing cure rates. Sonosensitizer-based sonodynamic therapy (SDT) exhibits traits such as non-invasiveness, localization on lesions, and deep tissue penetration, offering promising prospects for effective and low-toxicity treatment of malignant tumors [2–4].

The basic process of SDT involves utilizing ultrasound to activate sonosensitizers concentrated at the tumor site, generating reactive oxygen species (ROS) [5,6]. This process induces cancer cell apoptosis, inhibiting tumor development. Therefore, sonosensitizers capable of producing high levels of ROS under ultrasound irradiation are indispensable for effective SDT. Currently, sonosensitizers can be categorized into two main types: organic and inorganic sonosensitizers. Organic sonosensitizers, exemplified by porphyrin derivatives and phthalocyanines, exhibit a clear structure, good biocompatibility, and easy degradability in the body, albeit with structure instability during treatment. Further, the clinical application of organic sonosensitizers is constrained due to their inherent phototoxicity [7]. Compared to organic sonosensitizers, inorganic sonosensitizers represented by titanium dioxide (TiO_2) nanoparticles exhibit higher stability and are easily modifiable in morphology and structure. As a result, they have found widespread application in cancer SDT. Additionally, by integrating the imaging components into inorganic sonosensitizers, visual localization of the lesion can be achieved, contributing to enhancing therapeutic effectiveness [8]. However, the substantial band gap of TiO_2 nanoparticles, exemplified by the 3.2 eV in anatase, which is equivalent to the energy of ultraviolet light, leads to a reduced yield of ROS. Simultaneously, the metabolism problems and prolonged retention of TiO_2 nanoparticles in the body pose potential safety risks, collectively restricting their clinical application as sonosensitizers in SDT [9].

* Corresponding authors.
E-mail addresses: renwzh@nimte.ac.cn (W. Ren), aiguo@nimte.ac.cn (A. Wu).
[1] These authors contributed equally to this work.

https://doi.org/10.1016/j.cclet.2024.109727
1001-8417/

This review provides a concise summary of the fundamental mechanism underlying the application of TiO_2 in tumor SDT. Subsequently, it outlines the research progress in regulating the performance of TiO_2 sonosensitizers, encompassing factors such as morphology, particle size, structure, and the impact of the tumor microenvironment (TME) on sonosensitivity. Following this, the review discusses advancements in research on TiO_2-based multimodal treatments of tumors, including sonodynamic synergistic chemotherapy, photothermal therapy (PTT), chemical dynamic therapy, and immunotherapy. Then, a summary of research on imaging-guided TiO_2 SDT is presented. Finally, the review offers prospects for overcoming challenges in the clinical translation of TiO_2-based SDT, including enhancing the tumor enrichment of nanoparticles, addressing *in vivo* metabolism and excretion, and exploring synergies with immunotherapy.

2. The mechanism of TiO_2 in tumor SDT

During ultrasound propagation in the medium, it can induce mechanical, thermal, and cavitation effects, with widespread applications in tumor treatment, including drug delivery, focused ultrasound treatment, and SDT. In terms of drug delivery, the mechanical and cavitation effects induced by ultrasound can alter cell membrane permeability and enhance drug tissue penetration, thereby improving the therapeutic effectiveness in the treatment of solid tumors [10]. In clinical practice, focusing high-density ultrasound on the tumor site, leveraging thermal effects for rapid heating to above 65 °C, can lead to the ablation of the tumor. Additionally, focusing low-density ultrasound on the tumor site, through non-thermal mechanical effects, can rupture cancer cells to expose tumor antigens with intact structure, efficiently activating antitumor immunotherapy [11]. When it comes to SDT, the treatment mechanism is not yet clear, and the widely acknowledged mechanism involves ultrasonic cavitation effects [12]. The vibration of microbubble nuclei in a liquid under the action of ultrasound generates a series of dynamic processes known as ultrasonic cavitation. When the ultrasonic pressure reaches a certain threshold, the microbubbles rapidly expand, followed by sudden collapse. The collapse of the bubbles produces shockwaves, instantaneous high temperature, high pressure, and sonoluminescence, which are considered to play a role in the TiO_2-based SDT of tumors [13].

Depending on the intensity of the ultrasound, cavitation-generated microbubbles can exhibit different behaviors. At a lower intensity, the diameter of microbubbles oscillates within a specific range, causing acoustic streaming through medium movement, which is referred to as stable cavitation. At higher intensity, bubbles can expand beyond a critical size, leading to unstable growth and violent collapse, known as inertial cavitation. Both stable and inertial cavitation effects may result in some degree of mechanical damage to cancer cells in TiO_2-based SDT [14].

The cavitation refers to the nucleation, growth, and explosion of bubbles in water under ultrasound irradiation. The exploded bubbles can release significant energy through instantaneous shockwaves, high temperatures, and sonoluminescence. The shockwaves transmit pressure to the surrounding environment as high as 81 MPa. The high pressure can induce changes in the charge distribution of sonosensitizers, which interact with oxygen in the TME to generate ROS. The instantaneous high temperatures can reach 10,000 K and transfer to the surrounding TME. The temperature increase results in water decomposition, generating ·OH, which reacts with other endogenous substrates to produce ROS. Additionally, sonoluminescence can activate sonosensitizers to produce ROS. Although the current mechanisms are not fully understood, sonoluminescence is the most widely recognized mechanism in SDT [15].

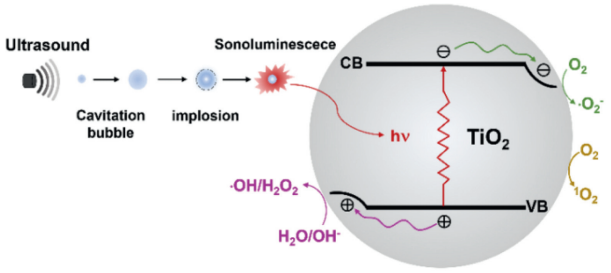

Fig. 1. Schematic mechanism of ROS production of TiO_2 under ultrasound irradiation.

Furthermore, the SDT of tumors with TiO_2 depends more on generating ROS induced by inertial cavitation and sonoluminescence. First, inertial cavitation can produce hydroxyl radicals from the ultrasonic decomposition (pyrolysis) of water vapor inside microbubbles, causing damage to cancer cells. Second, as shown in Fig. 1, sonoluminescence typically generates ultraviolet to blue light emission in water, coinciding with the excitation spectrum of TiO_2 [16]. For instance, anatase TiO_2 can be excited by ultraviolet light with a wavelength less than or equal to 387 nm. This excitation causes electrons in the valence band of TiO_2 to absorb the energy of photons and transition to the conduction band, creating photo-induced electrons; correspondingly, photo-induced holes form in the valence band, transforming oxygen in water or hydroxyl groups into singlet oxygen or hydroxyl radicals. The excitation of TiO_2 through sonoluminescence, leading to the generation of ROS, could be considered the primary mechanism behind inducing apoptosis in tumors in SDT. Excessive ROS can lead to mitochondrial damage and DNA injury, which causes apoptosis-related protein expression, such as the Bcl-2 and caspase family proteins, leading to cancer apoptosis [17].

3. Regulating the performance of TiO_2 sonosensitizers

To date, numerous research reports have explored the use of TiO_2 in SDT. The sonosensitivity of TiO_2 nanoparticles is primarily influenced by their bandgap, particle size, surface defects, and morphology [18–21]. For example, reducing the bandgap of TiO_2 enables lower energy ultrasound to excite free electrons more effectively, leading to the abundant generation of ROS for tumor cell destruction [22]. In addition, particle size determines the surface area and electronic structure of TiO_2. Smaller particles with a higher surface area-to-volume ratio increase the density of catalytically active sites [23]. In addition to tuning the properties of TiO_2 itself, optimizing the TME, including factors like oxygen levels and reducing components, can further amplify the effectiveness of SDT. Hence, this section summarizes the influence of TiO_2 morphology, structure, and regulation of the TME on its SDT efficacy.

3.1. Morphology regulation

In cancer SDT, when exposed to ultrasound irradiation, TiO_2 nanoparticles, serving as sonosensitizers, interact with substances such as H_2O, OH^-, and O_2 in tumor tissues. This interaction triggers the production of ROS, ultimately destroying tumor cells. A decrease in particle size significantly increases the specific surface area nanoparticles, enhancing interaction between ultrasound-generated free electrons (e^-) and holes (h^+) and surrounding substances, elevating ROS generation [24]. Additionally, the movement of electrons and holes in TiO_2 is influenced mainly by quantum confinement and transport control, with phononic characteristics significantly impacted by the geometric shape of the nanoparticles

[22]. Hence, alterations in TiO_2 particle size and morphology play a crucial role in influencing ultrasound treatment efficacy.

It has been found that when exposed to 1.0 W/cm^2 of ultrasound for 10 s, spherical TiO_2 nanoparticles with a diameter of 6 nm exhibited a remarkable killing efficiency exceeding 40% against melanoma cells [25]. To enhance the SDT effect of spherical TiO_2 nanoparticles, surface modifications were employed, incorporating drugs [26], cell membranes [27], targeting molecules [28], and even substances. These modifications not only extend the nanoparticles' circulation time within the body but also improve their intra-tumoral accumulation. Zhang *et al*. synthesized glutamine (GL)-coated TiO_{2-x} using the "sugar-coating theory". Through active GL uptake, these nanoparticles were targeted to cancer cells, increasing TiO_{2-x}@GL accumulation in tumors and enhancing ultrasound-based therapy for breast cancer [29].

Compared to spherical structures, mesoporous TiO_2 nanoparticles exhibit higher crystallinity and surface area, which not only can suppress the rapid recombination of electron-hole pairs but also provide more abundant surface sites. Additionally, mesoporous structures are suitable for loading drugs to improve treatment effectiveness. Wang *et al*. demonstrated a significant anticancer effect treated by mesoporous TiO_2 nanoparticles when exposure 1.5 W/cm^2 of ultrasound for 1 min, inducing 82.18% of apoptosis in liver cancer cells [30]. Chen *et al*. prepared polymer nanomedicines Fe(III)-artemisinin-loaded mesoporous TiO_2 nanoparticles for glutathione (GSH)-responsive chemodynamic therapy (CDT) and SDT, achieving a 67% cell-killing rate (0.7 W/cm^2; 10 min; 50% duty cycle) [31]. Moreover, hollow structures can provide more drug-carrying space. Shi *et al*. synthesized doxorubicin (DOX)-loaded and dsDNA surface-modified hollow mesoporous TiO_2 nanoparticles (MTNs-DNA), which the transmission electron microscope (TEM) images are displayed in Fig. S1A (Supporting information). Under ultrasound exposure, the TiO_2 nanoparticles generated $^1O_2$, leading to DNA cleavage and controlled release of DOX, thereby effectively treating drug-resistant tumors [32]. Compared to zero-dimensional nanoparticles, one-dimensional TiO_2 nanostructures, including nanorods and nanotubes, exhibit a high aspect ratio and a remarkable surface area-to-volume ratio. These features enable direct charge transfer and high electron mobility, showcasing broad SDT applications [33]. Wang *et al*. synthesized ultrafine structured polyethylene glycol (PEG)-TiO_{1+x}, which not only inhibited electron-hole recombination due to surface defects but also exhibited horseradish peroxidase activity. This unique characteristic enabled the efficient eradication of tumors by combining CDT and SDT [10]. As illustrated in Fig. S1B (Supporting information), the wall structure of nanotubes often contains various defects and has a larger specific surface area than rods. Sun *et al*. developed an ultrasound-enhanced antibacterial implant coating with gold nanoparticle-modified TiO_2 nanotubes named AuNPs-TNTs [34]. Figs. S2A and B (Supporting information) exhibits microstructure images of the nanotubes. The large area of the nanotubes increased Au loading, enhancing ROS production for efficient antibacterial treatment. These findings serve as a valuable reference for synthesizing high-performance sonosensitizers.

In addition, two-dimensional TiO_2 structures, attributing to their high carrier mobility granted excellent catalytic capabilities, have garnered attention in cancer SDT. Qiao *et al*. designed Pd-loaded black TiO_2 nanosheets, depicted in Fig. S2C (Supporting information) [19]. Under ultrasound exposure, TiO_2 nanosheets generated both ·OH and $^1O_2$, with Pd's peroxidase-like activity catalyzing OH into O_2, which further amplified the production of $^1O_2$ by TiO_2 in hypoxic conditions of the tumor, thereby achieving efficient tumor suppression. In conclusion, the diverse morphologies of TiO_2, ranging from mesoporous to one-dimensional and two-dimensional structures, present a spectrum of advantages in SDT. The unique attributes of each structure, such as high surface area, high carrier mobility, and drug-loading capacity, contribute to their effectiveness in treating cancers.

3.2. Structural modulation of TiO_2

There are three main crystal phases of TiO_2 nanoparticles: anatase, rutile, and brookite. However, only anatase is more suitable as a sonosensitizer due to lower oxygen adsorption capacity, slightly higher Fermi level, and higher hydroxylation degree. Consequently, anatase-phase TiO_2 nanoparticles are commonly employed in SDT [23]. When the excitation energy exceeds the band gap of TiO_2 (3.2 eV for anatase), electrons are excited from the valence band to the conduction band. The resulting free electrons and holes then migrate to the surface, where they interact with molecules like O_2, producing ROS. Competing with this charge transfer is the recombination of separated free electrons and holes on the surface of TiO_2, diminishing the efficiency of ROS generation [35]. Thus, reducing the bandgap energy and inhibiting the rapid recombination of electron-hole pairs are focal points for improving the efficacy of SDT. This section briefly overviews the modulation of band gap and electron-hole recombination through element doping and defect engineering and the enhancement of TiO_2's SDT effectiveness by regulating the TME.

3.2.1. Defect engineering

Due to the recombination of electron-hole pairs occurring in volume or surface defects, surface and volume defects play crucial roles in the activation process. Both surface and volume defects can serve as charge carrier traps and adsorption sites, where the transferred charges are traped to prevent electron-hole recombination. Consequently, enhancing the proportion of surface and volume defects can effectively increase active sites and reduce the bandgap [23]. When it comes to TiO_2 nanoparticles, they are mainly relative to surface defect engineering, attributing to the ROS produced on the surface of TiO_2 when under ultrasonic exposure. Enhancing surface defects in TiO_2 involves adjusting the Ti to O ratio, manipulating point defect concentrations, and introducing higher-valence ions as donors and lower-valence ions as acceptors [36]. Replacing ions of different sizes and charges by doping can cause deformation in the TiO_2 lattice, resulting in increased defects, such as oxygen vacancies and Ti^{3+} active sites. Under ultrasonic excitation, the generated electrons are efficiently captured, diminishing recombination rates, and thereby augmenting the sonosensitivity of TiO_2, as illustrated in Fig. S3 (Supporting information) [37]. The predominant strategy to enhance the surface defects of TiO_2 is primarily to employ a high-temperature reduction approach, such as hydrogenation [38].

Oxygen vacancies refer to the absence or migration of oxygen ions in the TiO_2 crystal lattice, which plays a multifaceted role in catalysis [39,40]. They introduce additional energy levels into materials and serve as specific reaction sites for certain molecules by acting as electron scavengers, facilitating the conversion of attached oxygen molecules into superoxide radicals. Furthermore, these vacancies induce changes in chemical rates based on the charge transfer of electrons or holes, ultimately enhancing the conductivity of materials. The conventional approach to augmenting oxygen vacancies is high-temperature reduction. Bian *et al*. prepared black TiO_{2-x} nanosheets using $NaBH_4$ as a reducing agent under 400 °C conditions. Their study identified the presence of Ti^{3+}, OH^-, and Ti-O, confirming the successful formation of oxygen vacancies. Although the crystal structure remained unchanged, the bandgap was reduced from 3.2 eV to 2.2 eV, as depicted Fig. 2A [41].

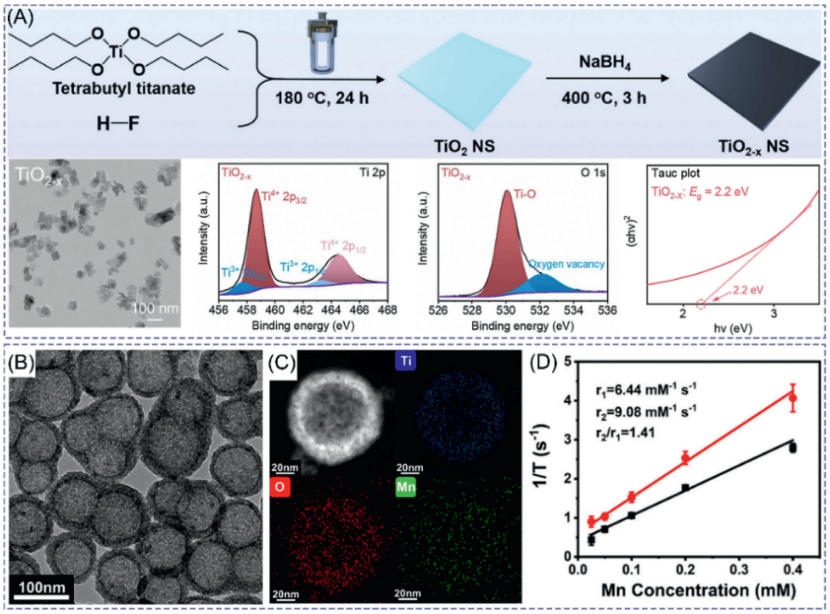

Fig. 2. (A) Synthesis route and performance characterization of black TiO_{2-x} nanosheets. Reproduced with permission [41]. Copyright 2023, Elsevier. (B–D) Morphology, magnetic resonance performance characterization of Mn-TiO_2. Reproduced with permission [48]. Copyright 2023, American chemical society.

3.2.2. Element doping

By replacing titanium or oxygen elements in TiO_2, doping is expected to maintain the integrity of the crystal structure and induce favorable changes in the electronic structure. Doping ions in TiO_2 act as traps for e^-/h^+ pairs, altering the recombination rate of charge carriers. Moreover, defects such as Ti^{3+} and oxygen vacancies, resulting from structural alterations, increase the density of active sites, thereby further enhancing catalytic activity [42]. The variance in charge states and ionic radii renders the replacement of Ti^{4+} cations in TiO_2 with other transition metal cations more feasible than substituting O_2 anions with other anions [43]. Doping with metal ions augments the light absorption capacity of TiO_2 by altering the electronic structure. Currently, various single metal ion doping have been studied to improve the catalytic performance of TiO_2, including manganese, iron, zirconium, tungsten, copper, molybdenum, lanthanides, and so on. Table S1 (Supporting information) provides a concise summary of the performance and applications of TiO_2 doped with various elements [44–56].

In the field of SDT, the doping of Mn and Fe elements has garnered considerable attention. These elements not only enhance the catalytic performance of TiO_2 but also can find applications in magnetic resonance imaging (MRI), enabling combined diagnosis and treatment. As shown in Figs. 2B–D, Yang *et al.* presented Mn-doped hollow TiO_2 nanoparticles, demonstrating a reduced bandgap of 3.0 eV. This modification led to a notable 1.3-fold increase in ultrasound-induced ROS production compared to the non-doped counterparts [48]. In addition, Mn-doped hollow TiO_2 nanoparticles were used as carriers to load ginsenoside Rk1, which cleverly inhibited glutaminase expression, blocking the synthesis of endogenous GSH in cancer cells. This reduced the consumption of ROS by the high GSH expression in the TME, leading to increased intracellular accumulation of ROS and significantly improving SDT efficacy in liver cancer. Additionally, the doping of Mn also endowed TiO_2 nanoparticles with good MRI performance, and the ratio of transverse relaxation rate to longitudinal relaxation rate was 1.41.

While studies on metal ion-doped TiO_2 have rapidly expanded into various applications like new electrodes, wastewater purification, and photodynamic therapy (PDT), their exploration in SDT still needs further development [57–59]. Building upon single-atom doping, co-doping two or more elements can further reduce the bandgap. Moreover, co-doping facilitates the replacement of elements in the TiO_2 lattice by promoting inter-element substitution. This increase in the element doping ratio further enhances the suppression of electron-hole recombination. Xu *et al.* co-doped Fe and Mo into TiO_2 nanoparticles, and compared with Fe-doped TiO_2, the bandgap energy was further reduced, demonstrating remarkable SDT performance. Meanwhile, the doping of elements resulted in dTiO_2 exhibiting peroxidase like (POD like) catalytic and glutathione peroxidase like (GPx like) activity, effectively alleviating tumor hypoxia and significantly consuming GSH to increase ROS levels [60].

3.2.3. Heterojunction composite structure

Developing heterojunctions presents a promising approach for enhancing the SDT performance of TiO_2 nanoparticles. These heterojunctions can be categorized based on material conductivity into two main types: semiconductor-semiconductor (S-S) and semiconductor-metal (S-M) heterojunctions [61]. According to the electron transfer mechanism, S-S heterojunctions can be further classified into I/II/III-type, p-n, and z-type. Notably, p-n and z-type heterojunctions demonstrate more effective electron-hole separation, longer charge carrier lifetimes, higher reaction rates, and broader spectral response [62]. Meanwhile, S-M heterojunctions include surface plasmon resonance effects and Schottky junctions [63].

Through efficient suppression of electron-hole pair recombination and formation of multiple reactive sites, heterojunctions maintain individual components' functionality and broaden substrate selectivity. Geng *et al.* constructed band-matched planar p-n heterojunction nanosheets using nitrogen-doped carbon dots (CD) as a p-type semiconductor and oxygen-deficient TiO_{2-x} as an n-type semiconductor [64]. Under ultrasonic irradiation, electrons generated in the CB of TiO_{2-x} are rapidly transferred to the VB of the p-type semiconductor, achieving spatial separation of electron-hole pairs and favoring the generation of more ROS. Thus, after low-dose ultrasound irradiation (50 kHz, 2.0 W/cm^2, 5 min), tumor-bearing mice exhibited a 100% survival rate over 50 days in the

nanosheets group, while the control group survived only 26 days [65]. Correspondingly, He *et al*. encapsulated a histone deacetylase inhibitor into hollow TiO_2 and surface-anchored graphitic carbon nitride quantum dots (g-C_3N_4, bandgap $\approx$ 2.7 eV), forming TiO_2@g-C_3N_4/RMD z-type heterojunction, as depicted in Fig. S4A (Supporting information) [66]. Electrons flow from a semiconductor with higher potential to one with lower potential upon contact, creating band bending and facilitating the forming of electron-hole pairs. Consequently, the formed z-type heterojunction effectively optimized the band structure of TiO_2 and enhanced the utilization of electron-hole pairs under high redox potentials during sonosensitization. Furthermore, the intrinsic peroxidase-like activity of g-C_3N_4 could react with endogenous H_2O_2, generating additional ROS to enhance SDT efficiency. These cutting-edge studies confirm the unprecedented potential of z-type heterojunctions as the next-generation sonosensitizers.

Furthermore, the TPG nano-reactor designed by Zhao *et al*. demonstrated the feasibility of using S-M heterojunctions [67]. The conductivity of noble metals in heterojunctions served as an electron mediator. In addition to separating electron-hole pairs through localized surface plasmon resonance, metals acted as mediators to transfer electrons from one CB to another, thereby increasing the oxidation–reduction potential for ROS generation. Therefore, compared to pristine TiO_2, the synthesized TiO_2@Pt Schottky structure promoted ROS generation under ultrasound irradiation. As shown in Fig. S4B (Supporting information), the efficient generation of $^1O_2$ and ·OH resulted from the rapid separation of electron-hole pairs and the clearance of holes by H_2O, attributing to the narrow electron bandgap and Pt acting as an electron trap. Moreover, decorated Pt exhibited robust simulated catalase-like activity, enhancing the combined therapeutic effect of SDT and starvation in tumors. In conclusion, by strategically constructing heterojunctions, it is possible to tune the band structure of sonosensitizers finely. This not only enhances substrate selectivity but also improves SDT performance, thereby advancing the field of TiO_2-based cancer treatment.

3.3. TiO_2-based sonosensitizers for TME regulation

Due to tumor cells' rapid proliferation and metabolism, the TME exhibits unique pathological and physiological characteristics compared to healthy tissues. The main features include a weakly acidic environment, high levels of GSH, severe hypoxia, overexpressed enzymes, and elevated ATP levels [68]. TME not only promotes the reproduction and metastasis of tumor cells but also resists the treatment of certain drugs, leading to drug resistance and treatment failure [69,70]. Therefore, regulating the TME is crucial for cancer therapy. TiO_2, as a sonosensitizer, possesses good chemical stability but lacks inherent responsiveness to the TME. However, this can be addressed by incorporating TME-responsive components with TiO_2. This approach shows promise for enhancing therapeutic effects [71]. The following section provides a summary of regulations concerning TiO_2-based sonosensitizers in the TME.

Numerous studies have shown that the elevation in extracellular acidity is a typical pathological characteristic of solid tumor tissues compared to the neutral environment of normal tissues [72]. This phenomenon, often called the Warburg effect, is characterized by a pH range of 6.5–6.8. For example, micelles composed of phospholipid polyethylene glycol polymers containing hydrazone bonds are relatively stable at pH 7.4 but undergo hydrazone bond cleavage within a few hours under pH 6.5 or lower conditions [73]. In addition to mild acidity in the TME, the pH values in the cytoplasmic lysosomes and endosomal compartments experience a notable decrease, ranging from 6.5 to 4.5 [74]. This difference in acidity can be used as a promising endogenous stimulus for the development of weakly acidic-responsive nanoparticles. As illustrated in Fig. S5 (Supporting information), TiO_2@CaP nanoparticles designed by Tan *et al*. could decompose into TiO_2 and Ca^{2+} when exposed from physiological neutrality to the pathological tumor acidic environment. This switch from a "closed" to an "open" state induced ROS generation and Ca^{2+} overload, amplifying the rate of cancer cell apoptosis [75].

In addition to the acidic microenvironment, elevated GSH levels are also a characteristic of the TME. GSH, a tripeptide containing γ-glutamyl bonds and sulfhydryl groups composed of glutamic acid, cysteine, and glycine, is critical in maintaining cellular redox balance [76]. According to reports, the concentration of GSH inside cancer cells ($5–10 \times 10^{-3}$ mol/L) significantly exceeds that in normal cells ($1–5 \times 10^{-3}$ mol/L). This heightened level is attributed to the high catalytic activity of cytoplasmic enzyme GSH reductase and nicotinamide adenine dinucleotide phosphate in cancer cells, facilitating the reduction of oxidized GSH to GSH [77]. Since oxidative ROS can react with reducing GSH, reducing the intracellular GSH content and inhibiting GSH synthesis are effective methods to enhance TiO_2 SDT effects [78]. Our team recently synthesized Mn-doped hollow TiO_2 nanoparticles loaded with ginsenoside Rk1 (Rk1@MHT-PEG). Rk1 demonstrated the ability to impede glutaminase expression, thereby inhibiting GSH synthesis. This, in turn, led to a reduction in ROS consumption due to the decreased GSH levels in the TME, ultimately augmenting the efficacy of SDT [48]. Additionally, Li *et al*. designed a TiO_{2-x}@Cas9-NH@HA based on hypoxic TiO_{2-x} in response to TME. In the TME, overexpressed hyaluronidase and GSH could disrupt hyaluronic acid (HA) and disulfide bonds, releasing Cas9/sgRNA from TiO_{2-x}. This system targeted stress mitigation factors, nuclear factor E2-related factor 2 (NRF2), and heat shock protein 90α (HSP90α), thereby reducing the stress tolerance of tumor cells [79].

Furthermore, hypoxia stands out as another prominent characteristic in most tumors [80]. To adapt to the rapid growth of tumors, irregular microvessels are formed at tumor sites to provide sufficient nutrients for tumor cells. However, significant oxygen consumption impedes cellular metabolic activities, leading tumor cells to adjust to a hypoxic environment through a cascade of hypoxia-inducible factors (HIF), primarily HIF-1. This hypoxic adaptation alters the general biochemical environment around cells and affects cellular energy metabolism [81–83]. SDT relies on the presence of oxygen to generate ROS. However, the hypoxic conditions within the TME limit the production of ROS [84]. Therefore, hypoxia can serve as a target for the tumor-specific activation of prodrugs, designing a series of nanocarriers to deliver hypoxia-activated prodrugs. For example, Li and colleagues developed RBC-mTNPs@AQ4N nanoparticles for AQ4N drug delivery to tumors [85]. The hypoxic environment of the tumor site activated the AQ4N drug into a toxic product that damaged tumor cells. Additionally, improving the hypoxic conditions of the TME can enhance SDT effects. For instance, the self-cascade nanoenzyme platform HABT-C@HA designed by Tao *et al*. could generate oxygen to alleviate hypoxia and produce ROS, schematically illustrated in Fig. S6 (Supporting information) [86].

4. TiO_2 nanoparticle-based ultrasound treatment in cancer

The summary of SDT and SDT combined therapy using TiO_2-based nanomaterials is provided in Table S2 (Supporting information) [19,27,29,30,45,49,65,67,75,85–105,107].

4.1. SDT

As discussed in the primary mechanism of SDT from the above section, there are three crucial elements for efficient SDT: excitation source, sonosensitizer, and O_2 level in tumors [108,109]. In the pursuit of advancing cancer treatment, considerable research has

been dedicated to the development of highly effective sonosensitizers to amplify the efficacy of SDT. This section aims to present a comprehensive overview of the recent advancements made in utilizing TiO_2 for cancer SDT within the last five years.

SDT exhibits significant advantages over PDT in terms of tissue penetration depth. However, the oxygen-dependent Type II SDT is severely limited by the hypoxic conditions of the TME. Therefore, it is crucial to develop sonosensitizers that possess the ability to continuously and reliably generate ROS even in hypoxic conditions (Type I SDT). Cao *et al*. designed sheet-like TiO_2/C nanocomposites derived from metal-organic frameworks carbon structures [65]. As illustrated in Fig. S7 (Supporting information), they found that the TiO_2/C nanocomposites are hypoxia-tolerant and can stably generate a large amount of ROS, thereby achieving efficient Type I SDT. Under repeated ultrasound irradiation, the nanocomposites continuously produced ROS, inducing DNA damage and apoptosis in tumor cells *in vitro* and *in vivo*. Another notable characteristic of TME is the high concentration of the reducing GSH, which can consume the oxidative ROS produced by sonosensitizers, thereby limiting the SDT efficacy. Guan *et al*. designed Nb_2C nanosheets to accommodate TiO_2 sonosensitizers and L-buthionine-sulfoximine (BSO) [87]. Their experimental results showed that the TiO_2-based nanocomposites could reduce ROS consumption by inhibiting GSH synthesis. Additionally, the Nb_2C nanosheets enhanced the generation and separation of electron-hole pairs, indicating that the prepared nanocomposites could intervene in the normal metabolism pathways of ROS and GSH, disrupt redox balance, and reshape the TME.

4.2. Combination of SDT and CDT

CDT, proposed by Bu and colleagues in 2016, is a novel cancer treatment strategy that precise generation of ·OH in tumor regions through Fenton or Fenton-like reactions, inducing cancer cell apoptosis [106]. However, the CDT efficacy is limited due to the low levels of endogenous H_2O_2 in TME, resulting in minimal generation of ·OH through Fenton or Fenton-like reactions, as depicted in Fig. S10 (Supporting information). Additionally, high levels of GSH in the TME can rapidly eliminate ·OH. Therefore, combining SDT and CDT to elevate ROS concentration has significantly enhanced therapeutic efficacy [110].

Recently, Chen *et al*. designed single copper atom-doped TiO_2 nanosensitizers with highly catalytic and sonodynamic activity for synergistic CDT and SDT in triple-negative breast cancer [50]. As displayed in Fig. 3, the single copper atoms were precisely anchored at the most stable titanium vacancies of hollow TiO_2 sonosensitizers . This strategic configuration resulted in a noteworthy augmentation of the catalytic activity in copper-mediated Fenton-like reactions. Concurrently, it fostered the separation of electron-hole pairs, leading to a substantial improvement in the sonosensitivity performance of TiO_2. The *in vivo* results demonstrated that the engineered single-atom-doped sonosensitizers effectively inhibited triple-negative breast cancer. Similarly, Bai *et al*. synthesized iron-doped ultra-small TiO_2 nanodots, and the introduction of Fe resulted in enhanced sonosensitivity under ultrasound irradiation compared to pure TiO_2 nanodots [49]. Moreover, these engineered nanodots demonstrated the capability of amplifying ROS production by Fenton reactions, thereby achieving a synergistic therapeutic effect of CDT and SDT. To address the issue of low H_2O_2 levels in the TME leading to insignificant CDT effects, researchers considered endowing nanosensitizers with the ability to generate H_2O_2 at tumor sites. Besides, titanium-based MXene materials have also been applied to cancer SDT. Zhang *et al*. prepared two-dimensional nanosensitizer/nanocatalyst Ti_3C_2/CuO_2@BSA nanocomposites, achieving high-performance and synergistic tumor SDT and CDT in response to the TME [111]. CuO_2 nanoparticles integrated with Ti_3C_2 MXene enabled *in situ* generation of H_2O_2 in the acidic TME, oxidizing Ti_3C_2 to prepare TiO_2 nanosensitizers. This process, combined with the heightened separation of electron-hole pairs facilitated by the carbon-based substrate post-oxidation, notably enhanced the efficiency of SDT. Concurrently, the ultrasonic radiation in the sonodynamic process bolstered copper-induced Fenton-like reactions, increasing the production of ROS and enhancing synergistic SDT and CDT in tumors.

4.3. SDT combined with PTT

PTT is a widely employed treatment approach that entails the targeted ablation of tumors by inducing localized heat through laser irradiation of photothermal agents concentrated within the tumor region [112]. Due to the correlation between the wavelength in PTT and tissue penetration depth, many researchers are exploring photothermal agents that can be excited in the near-infrared-II area, spanning from 1000 nm to 1350 nm. This specific range allows for deeper tissue penetration, reaching depths of up to 3 cm [113]. *In vivo* studies have revealed that successful PTT treatment often requires high-power density laser irradiation and prolonged exposure. Unfortunately, such conditions can result in significant damage to surrounding healthy tissues. Tumors not exposed to such intense irradiation may experience recurrence, as the treatment may not achieve complete eradication. Given that PTT is an oxygen-independent treatment method and the mild photothermal effect its produces can alleviate the hypoxia in TME by promoting vasodilation, there is a growing interest in exploring the combined

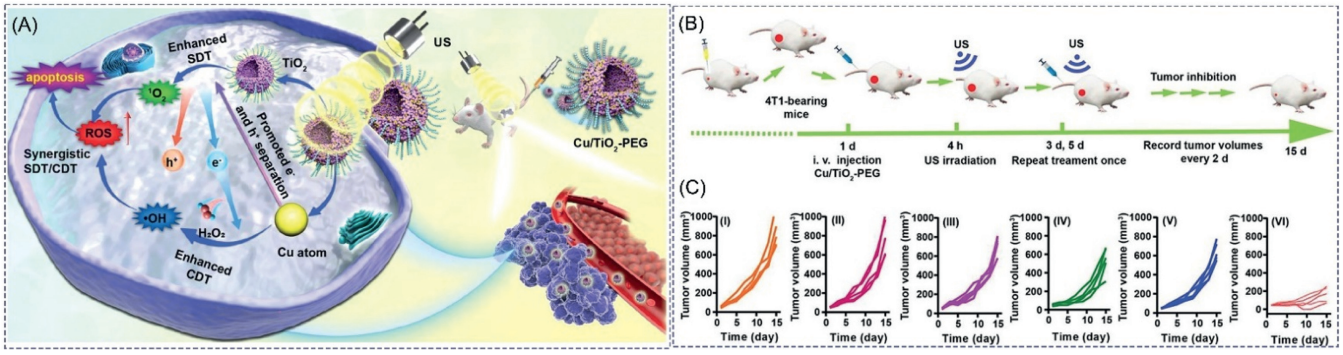

Fig. 3. (A) Schematic illustration of Cu/TiO_2-PEG application in SDT and CDT of cancer. (B) Schematic diagram of the establishment of 4T1 tumor-bearing mice and evaluation of the therapeutic effect. (C) Individual tumor growth curve of mice after different treatments. I: control, II: only US, III: TiO_2-PEG, IV: TiO_2-PEG +US, V: Cu/TiO_2-PEG, VI: Cu/TiO_2-PEG + US. Reproduced with permission [50]. Copyright 2023, John Wiley and Sons.

application of SDT and PTT as a feasible approach for cancer therapy [92].

Shen *et al*. proposed a nanoplatform that integrated black TiO_2 nanoparticles with an iridium complex and functionalized cancer cell membranes for layered targeting, synergistic photothermal and sonodynamic cancer imaging, and treatment [90]. As shown in Fig. S8 (Supporting information), nanoplatform could effectively generate heat under laser irradiation and catalyze ROS production under ultrasound exposure. The nanoparticles were selectively located in mitochondria, preferentially accumulating in cancer cells rather than normal cells. Under the co-irradiation of a 1064 nm laser and ultrasound, the nanoparticles functioned as dual agents, serving both as imaging agents for identifying tumor sites with high spatial resolution and therapeutic agents, ultimately achieving complete tumors eradication in the mouse model. This combined treatment method effectively compensated for the poor SDT performance caused by hypoxia, utilizing the NIR-II excited PTT therapy. Similarly, Du *et al*. successfully constructed black phosphorus nanosheets loaded with hypoxia-inducing black TiO_2 for synergistic PTT and SDT [93]. The black TiO_2 provided efficient SDT performance, while the black phosphorus nanosheets endowed the composite material with a heightened photothermal conversion efficiency of 44.1%. Zhang *et al*. synthesized GL-wrapped TiO_{2-x} nanoparticles for combined PTT and SDT in breast cancer [29]. The introduction of GL significantly enhanced the targeting capability of the nanoparticles. Moreover, the TiO_{2-x} nanoparticles, with a defect structure prepared by aluminum reduction, exhibited notable SDT and PTT effects.

4.4. SDT combined with chemotherapy

Chemotherapy, as one of the traditional cancer treatment methods, meets the obstacle of severe side effects such as organ toxicity and immunosuppression and ultimately leads to patient death from recurrence or treatment-related complications [113,114]. Currently, there is a growing development of TiO_2 nanosensitizers with specific structures, such as mesoporous or hollow configurations, serving as drug carriers. Chemotherapeutic drugs can be loaded into their surface pores or large cavities. During the combined SDT treatment, chemotherapy drugs are precisely delivered to the tumor site, thereby mitigating a range of adverse reactions. Additionally, many researchers utilized the specific hypoxic environment of the TME to deliver hypoxia-activated prodrugs using nanosensitizers. Ning *et al*. engineered C-TiO_2/TPZ@CM for engineered SDT and hypoxia-activated chemotherapy. The design incorporated a core-shell structure featuring a hollow TiO_2 loaded with tirapazamine (TPZ) as the core, surrounded by a cancer cell membrane (CM) serving as the outer shell [27]. As shown in Fig. S9 (Supporting information), the C-TiO_2/TPZ@CM not only achieved tumor targeting through homologous binding but also acted as nanosensitizers to kill cancer cells under ultrasound irradiation. The oxygen consumption induced by SDT created a hypoxic environment, thereby activating the co-delivered TPZ for enhanced therapeutic effects. Similarly, Li *et al*. designed a biomimetic drug delivery system that combined SDT with hypoxia-targeted chemotherapy [85]. In this system, red blood cell membrane-coated mesoporous TiO_2 nanoparticles (RBC-mTNPs) efficiently delivered the hypoxia-activated prodrug banoxantrone hydrochloride (AQ4N). Upon ultrasound activation, mesoporous TiO_2 nanoparticles acted as a sonosensitizer, generating ROS, inducing cell apoptosis, and disrupting the RBC membrane. This resulted in ultrasound-mediated on-demand release of AQ4N. When activated under hypoxia, AQ4N transformed into toxic products, achieving a synergistic approach of combined SDT and hypoxia-targeted chemotherapy for breast cancer.

4.5. SDT combined with immunotherapy

In recent years, cancer immunotherapy has emerged as a promising strategy to stimulate the innate immune system to recognize, attack, and eliminate tumor cells with minimal damage to healthy cells [115]. Its notable advantage lies in its capacity to leverage the body's immune system to specifically target and kill cancer cells without requiring external drugs [116]. Cancer immunotherapy encompasses various forms, including targeted antibodies, cancer vaccines, adoptive cell therapy, oncolytic viruses, immune checkpoint inhibitors, cytokines, and immunoadjuvants. However, most of these immunotherapy strategies benefit only a tiny fraction of patients and may induce systemic autoimmune side effects in some cases.

It has been established that the process by which tumor cells undergo non-immunogenic to immunogenic transformation upon external stimuli, leading to initiating an antitumor immune response, is known as immunogenic cell death (ICD). Modalities such as radiotherapy, PDT, PTT, and SDT can induce tumor cell death, releasing tumor-associated antigens and pro-inflammatory cytokines, activating dendritic cells and cytotoxic T cells to eliminate cancer cells. ICD not only directly kills cancer cells but also induces an antitumor immune response targeting a wide range of solid tumors. This vaccination-like strategy is employed to convert the "cold" TME into an immunogenic "hot" TME. Therefore, integrating immunotherapy with SDT strategy, utilizing ROS generation to trigger ICD, presents a promising approach for restraining tumor development and achieving superior therapeutic outcomes [117]. Tao *et al*. devised a multifunctional platform using gold nanoparticles and carbon dot-modified hollow black TiO_2 nanospheres (HABT-C) with cascaded enzyme activity [86]. This platform aimed to reverse immune suppression and alleviate hypoxia within TME. Hollow black TiO_2 demonstrated efficient SDT capability, and HABT-C@HA was suggested to reverse immune suppression, enhancing the therapeutic effects of ICD. Similarly, Lu *et al*. designed a multifunctional sonosensitizer named $Au_{S/C}$-TiO_2 composed of Au single atoms and clusters, with the goal of enhancing SDT and glucose consumption [97]. The immune cell analysis *in vivo* confirmed the effectiveness of the $Au_{S/C}$-TiO_2 sonosensitizers in inducing antitumor immune responses. Therefore, the improved generation of ROS and intense endoplasmic reticulum stress ultimately led to potent ICD, inhibiting 80% of tumor cells. This study suggests that the simultaneous presence of ROS generation and intense endoplasmic reticulum stress can effectively trigger a robust ICD-mediated immune response.

All of these aspects fall within the realm of the material itself modulating the immune system under ultrasound activation, as outlined in this research. Tan and colleagues introduced a deformable core-shell TiO_2@CAP sonosensitizer [75]. In the acidic TME activated by ultrasound, it reactivated the generation of ROS and dissolved its cap shell to release calcium ions. TiO_2 significantly enhanced ICD, thereby promoting the recruitment and infiltration of T cells into immunologically cold tumors. When integrated with programmed cell death protein-1 (PD-1) checkpoint blockade therapy, SDT-mediated by TiO_2@CAP induced systemic antitumor immunity, leading to regression of untreated distant tumors and suppression of lung metastasis. Moreover, programmed cell death ligand 1 antibody (APDL1) can specifically bind to programmed cell death-ligand 1 (PD-L1) expressed on tumor cells, exerting as an immune checkpoint in the tumor immune microenvironment. By competitively inhibiting the interaction between programmed cell death 1 and PD-L1, it enhanced the effector function of $CD8^+$ T cells. Wei *et al*. developed a novel TiO_2 based sonosensitizer loaded with malignant melanoma cell membrane (B16F10M) and programmed cell death-ligand 1 antibody (aPD-L1) for dual-targeted enhancement of cancer SDT [99]. Under ultrasound irradi-

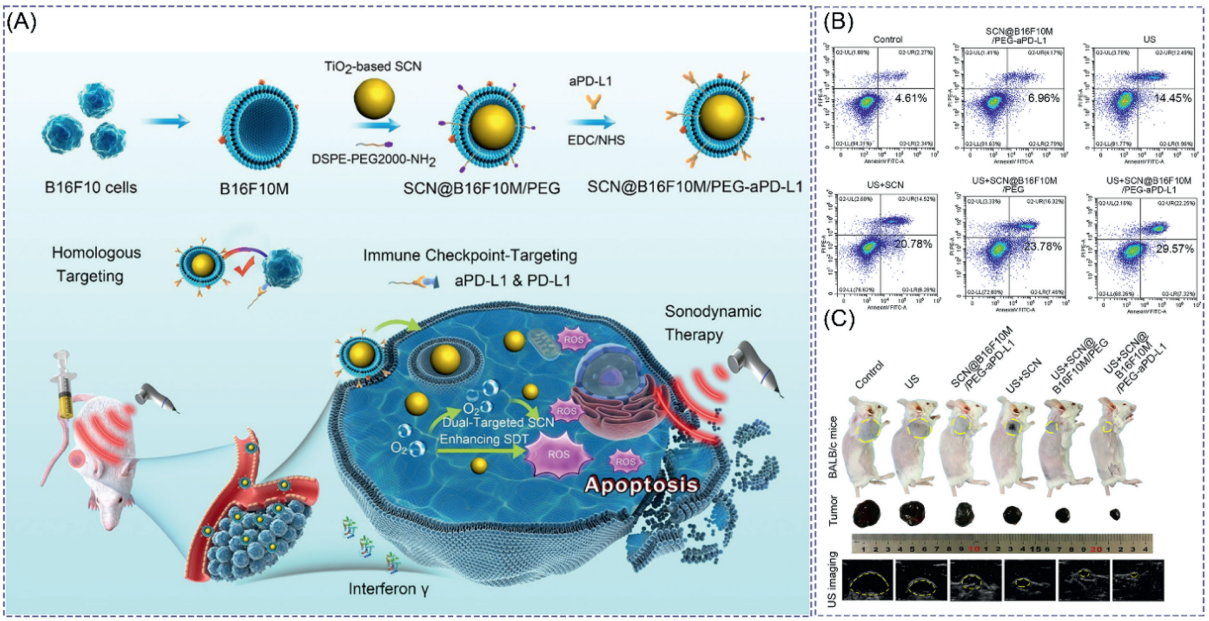

Fig. 4. (A) Schematic illustration of homology and immune checkpoint dual-targeted and enhanced SDT of tumors by SCN@B16F10M/PEG-aPD-L1. (B) Flow cytometry (FCM) detection of the apoptosis of B16F10 cells. (C) Photographs and tumor images of BALB/c mice. Reproduced with permission [99]. Copyright 2021, American Chemical Society.

ation, showcased in Fig. 4, the synthesized SCN could catalyze substantial generation of O_2. *In vivo* and *in vitro* experiments demonstrated that the functionalized sonocatalytic nanoagents possessed dual homologous and immune checkpoint targeting capabilities, achieving an enhanced therapeutic effect in combined SDT and immunotherapy.

4.6. Treatment visualization

Currently, various imaging modalities have been employed for TiO_2-based imaging-guided tumor treatments, including ultrasound imaging, MRI, computed tomography (CT), photoacoustic imaging (PAI), and multimodal Imaging. These imaging techniques have been widely applied in clinical settings, enabling the preoperative, intraoperative, or postoperative monitoring of pathological conditions within patients [118–121]. They provide physicians with precise, high-resolution images in both temporal and spatial dimensions, achieving an integrated approach to diagnosis and treatment. The following section summarizes the advances in exploring using TiO_2-based sonosensitizers to visualize cancer SDT.

Ultrasound has been widely utilized in clinical settings for cancer detection and image-guided tissue biopsies [122]. Carbon fluorine compounds stabilized microbubbles have long been employed as contrast agents for clinical ultrasound imaging. Considering the benefits of nano-bubbles for targeted tumor penetration, the advancement of ultrasound contrast agents using nano-sonosensitizers holds significant promise for both tumor diagnosis and treatment [123]. Feng *et al.* synthesized hollow mesoporous TiO_2 sonosensitizers (HMTNPs) loaded with TPZ and modified with *S*-nitrosothiol (R-SNO) [124]. Upon ultrasound stimulation, the sonosensitizers released ROS and, concurrently, could selectively release NO on demand, as illustrated in Figs. 5A and B. The echogenic properties of NO made the sonosensitizers suitable as a contrast agent for improving ultrasound imaging.

MRI represents a significant advancement in medical imaging. The fundamental principle involves using radiofrequency pulses to excite hydrogen nuclei within the body, inducing resonance and energy absorption [125]. After the radiofrequency pulses cease, hydrogen nuclei emit radiofrequency signals at specific frequencies, releasing the absorbed energy. These signals are then captured by external receivers and undergo processing by electronic computers to generate images. Contrast agents used for MRI are categorized into longitudinal relaxation (T_1) agents and transverse relaxation (T_2) agents based on their underlying principles. T_1 contrast agents operate by directly interacting with hydrogen nuclei in water molecules and paramagnetic metal ions, leading to a shortening of T_1, enhancing the signal and resulting in brighter images. On the other hand, T_2 contrast agents disrupt the external magnetic environment, causing rapid dephasing of neighboring hydrogen protons during relaxation, resulting in weaker signals and yielding darker images [126]. The doping of magnetic metal elements, including Fe, Mn, and Gd, not only reduces the bandgap of TiO_2 but also provides MRI performance. As displayed in Fig. 5D, Bai *et al.* synthesized Fe-doped TiO_2 nanoparticles, and after administration in tumor-bearing mice for 24 h, a noticeable enhancement was observed at the tumor site, indicating enhanced MRI contrast effect [49]. Similarly, our team synthesized bTiO_2-Gd-IGF1-GEM showed a significant brightening MRI effect in tumors of mice models [127].

CT imaging is characterized by its rapid speed, high resolution, cost-effectiveness, and non-invasiveness, playing a crucial role in disease diagnosis, and has been widely used in clinics. While CT can effectively image lung and bone samples directly, contrast agents are required for imaging soft tissues due to the lack of inherent contrast [128]. Nanoparticle contrast agents, especially those containing iodine or gold nanoparticles, have been widely used in micro-CT imaging, as the kidneys do not rapidly clear them. Therefore, combining TiO_2 with SDT effects and CT imaging represents a promising approach for cancer treatment and the imaging is shown in Figs. 5E and F [102].

PAI combines the principles of optics and acoustics, utilizing laser pulses to irradiate samples. Upon absorption of laser energy, the sample undergoes rapid thermal expansion, generating acoustic signals. These signals are captured by detectors and converted into images, forming a photoacoustic image [129]. PAI presents several advantages over traditional techniques, including enhanced imaging depth, high resolution, rapid imaging speed, and minimal im-

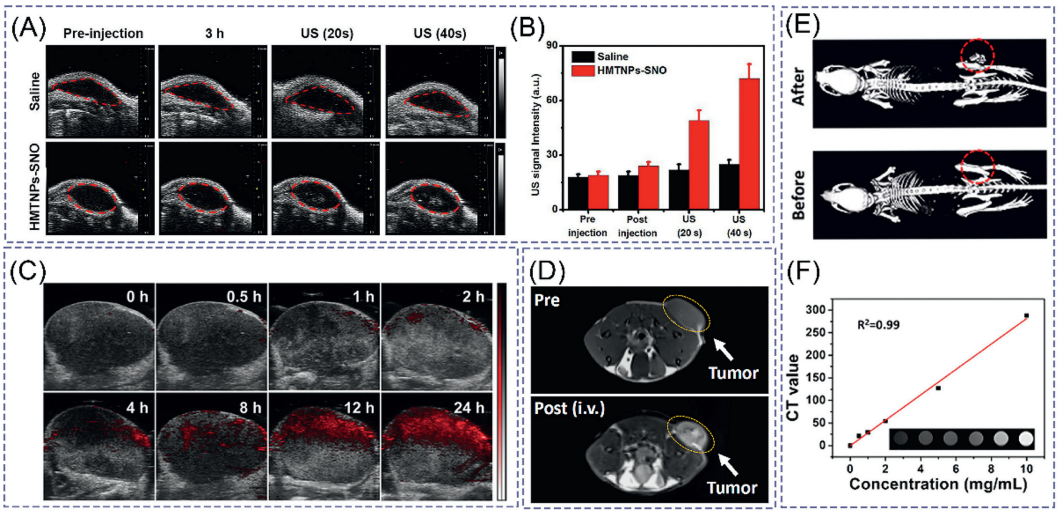

Fig. 5. TiO_2 based nanomaterials for cancer imaging. (A) TPZ-HMTNPs-SNO developed for ultrasound (US) imaging and (B) its signal intensity profile. Reproduced with permission [124]. Copyright 2018, John Wiley and Sons. (C) Photoacoustic (PA) images of tumor after injection of Nb_2C/TiO_2/BSO-PVP. Reproduced with permission [87]. Copyright 2020, John Wiley and Sons. (D) MRI of tumor-bearing mice before and after injection of Fe-TiO_2 NDs. Reproduced with permission [49]. Copyright 2020, John Wiley and Sons. (E) CT images of a mouse taken before and after intravenous injection of Au-TiO_2-A-TPP. (F) CT images and the value of CT signal of Au-TiO_2-A-TPP. Reproduced with permission [102]. Copyright 2019, American Chemical Society.

pact on biological tissues [130]. Given these advantages, integrating PAI with TiO_2 SDT is highly desirable. Due to the excellent PAI performance of Nb_2C itself, Guan *et al.* prepared Nb_2C/TiO_2/BSO-PVP sonosensitizer, as shown in the Fig. 5C, PAI was used to track the accumulation of Nb_2C/TiO_2/BSO-PVP within tumors over 24 h. It was observed that the photoacoustic signal within the tumor gradually increased over time [87].

Although TiO_2-based sonosensitizers have made significant progress in single-modal imaging, each imaging modality alone is not sufficient to achieve high resolution and accuracy. Therefore, complementary imaging modes are employed to compensate for the deficiencies between individual imaging modalities [131]. To endow TiO_2 with multimodal imaging capabilities, functional components with other imaging characteristics can be loaded or doped into TiO_2 due to their excellent feasibility and ease of surface chemical modification. He *et al.* synthesized mesoporous TiO_2 nanoparticles ($mTiO_2$s) loaded with honokiol (HNK) and combined them with the photothermal material polypyrrole (PPY) [91]. Both $mTiO_2$ and $mTiO_2$@PPY exhibited intense ultrasound and PAI capabilities. The signals gradually increased with increasing concentration, demonstrating their enhanced multimodal imaging capabilities.

5. Conclusions

This article comprehensively reviews the representative and latest research progress in the sonodynamic mechanism, performance regulation, tumor SDT, and visualization treatment of TiO_2-based sonosensitizers. Firstly, the mechanism and advantages of ultrasound therapy in cancer treatment applications are introduced. Then, it discusses how to optimize the performance of TiO_2, including the control of morphology and particle size, metal or nonmetal doping, defect engineering, and heterojunction structure. The review also summarizes the strategies to enhance the therapeutic effects of TiO_2 in tumor treatment through the modulation of the TME. In terms of therapeutic applications, the article reviews the TiO_2-based tumor SDT and its combination with other treatment modalities, such as PTT, CDT, chemotherapy, and immunotherapy. Finally, it summarizes the application of TiO_2 and imaging techniques for treatment visualization. Although significant progress has been made in the performance regulation of TiO_2, some challenges and issues should be further addressed.

The primary hurdle that must be addressed is the extended retention of TiO_2 in the body over the long term. Although numerous TiO_2 nanoparticles with ultra-small particle sizes have been designed, demonstrating good biocompatibility and the ability to be metabolized and excreted, the process of nanoparticles within the body is highly intricate. It involves being enveloped by protein coronas and subsequently being engulfed by immune cells, leading to a series of uncertain immune reactions or long-term toxicity risks. Therefore, more efforts are needed to elucidate the fate of TiO_2 within the body and specific immune response issues. Second, the mechanism of the sonosensitivity of TiO_2 is still unclear. Further study of the sonoluminescence effect mechanism is crucial for designing high-performance sonosensitizers. Third, enhancing the accumulation of TiO_2 sonosensitizers at the tumor site is crucial. Although TiO_2 sonosensitizers have been demonstrated excellent tumor therapeutic performance, the amount reaching the tumor site after intravenous injection is still shallow. Therefore, it is essential to design more biocompatible TiO_2 sonosensitizers with long cycle and low immunogenicity to avoid rapid clearance. Finally, immunotherapy can eliminate cancer by activating the host's immune system. Ultrasound has been proven to enhance immune activation in the TME. Therefore, the combination of SDT and immunotherapy has broad clinical prospects.

Declaration of competing interest

The authors declare that they have no known competing financial interests or personal relationships that could have appeared to influence the work reported in this paper.

Acknowledgments

This work was supported by the National Natural Science Foundation of China (Nos. 31971292, 32025021, 32171359, 32111540257, 32311530040), the Zhejiang Province Financial Supporting (No. 2020C03110), and the Key Scientific and Technological Special Project of Ningbo City (Nos. 2020Z094, 2023Z189).

Supplementary materials

Supplementary material associated with this article can be found, in the online version, at doi:10.1016/j.cclet.2024.109727.

References

[1] R.L. Siegel, K.D. Miller, N.S. Wagle, A. Jemal, CA Cancer J. Clin. 73 (2023) 17–48.
[2] X.J. Qin, B.W. Ding, X.Y. Zhang, et al., J. Biomater. Tissue Eng. 12 (2022) 665–672.
[3] B.Y. Chu, Y. Qu, C. He, Z.Y. Qian, Mater. Express 12 (2022) 1277–1286.
[4] Z.J. Wang, L.L. Chi, Chin. Chem. Lett. 29 (2018) 11–18.
[5] J.X. Ding, J.J. Chen, L.Q. Gao, et al., Nano Today 29 (2019) 100800.
[6] T. Luo, K.Y. Zhang, L.Y. Zhao, et al., Mater. Express 10 (2020) 883–891.
[7] J.L. She, X.F. Zhou, Y.J. Zhang, et al., Adv. Healthc. Mater. 10 (2020) 2001208.
[8] C. Dong, Q.Z. Jiang, X.Q. Qian, et al., Nanoscale 12 (2020) 5587–5600.
[9] A. Maleki, M. Seyedhamzeh, M. Yuan, et al., Small 19 (2023) 2206253.
[10] X.W. Wang, X.Y. Zhong, L.X. Bai, et al., J. Am. Chem. Soc. 142 (2020) 6527–6537.
[11] Y. Chen, H.R. Chen, J.L. Shi, Adv. Healthc. Mater. 4 (2014) 158–165.
[12] S. Liang, X.R. Deng, P.A. Ma, et al., Adv. Mater. 32 (2020) 2003214.
[13] W.J. Chen, J. Wang, L. Cheng, et al., ACS Appl. Bio Mater. 4 (2021) 1483–1492.
[14] C.C. Chen, P.S. Sheeran, S.Y. Wu, et al., J. Control. Release 172 (2013) 795–804.
[15] S.B. Son, J.H. Kim, X.W. Wang, et al., Chem. Soc. Rev. 49 (2020) 3244–3261.
[16] D. Song, W. Xu, M. Luo, et al., Nanoscale 13 (2021) 14130–14138.
[17] H.S. Tuli, J. Kaur, K. Vashishth, et al., Arch. Toxicol. 97 (2022) 103–120.
[18] L.F. Chen, P.Y. Xu, S.B. Wang, A.Z. Chen, Chin. Sci. Bull. 66 (2021) 1057–1066.
[19] X.H. Qiao, L.Y. Xue, H. Huang, et al., J. Nanobiotechnol. 20 (2022) 186.
[20] Y. Wang, Y.M. He, Q.H. Lai, M.H. Fan, J. Environ. Sci. 26 (2014) 2139–2177.
[21] L.B. Xiong, J.L. Li, B. Yang, Y. Yu, J. Nanomater. 2012 (2012) 831524.
[22] A.G. Wu, W.Z. Ren, TiO_2 Nanoparticles: Applications in Nanobiotechnology and Nanomedicine, Wiley-VCH Verlag GmbH & Co. KGaA, Weinheim, 2020.
[23] X.B. Chen, S.S. Mao, Chem. Rev. 107 (2007) 2891–2959.
[24] T. Rajh, N.M. Dimitrijevic, M. Bissonnette, et al., Chem. Rev. 114 (2014) 10177–10216.
[25] Y. Harada, K. Ogawa, Y. Irie, et al., J. Control. Release 149 (2011) 190–195.
[26] Y. Chen, Y. Wan, H.J. Zhang, Z.J. Jiao, Int. J. Nanomed. 6 (2011) 2321–2326.
[27] S.P. Ning, X.L. Dai, W.W. Tang, et al., Acta Biomater. 152 (2022) 562–574.
[28] S. Shen, X.M. Guo, L. Wu, et al., J. Mater. Chem. B. 2 (2014) 5775–5784.
[29] L. Zhang, P.F. Zhu, T. Wan, et al., Front. Bioeng. Biotechnol. 11 (2023) 1139426.
[30] X. Wang, W.P. Wang, L.D. Yu, et al., J. Mater. Chem. B 5 (2017) 4579–4586.
[31] J. Chen, J. Zhang, X. Wei, et al., J. Colloid Interface Sci. 650 (2023) 1773–1785.
[32] J.J. Shi, W. Liu, Y. Fu, et al., J. Control. Release 274 (2018) 9–23.
[33] Y.R. Li, S. Wang, Y.J. Dong, et al., Bioact. Mater. 5 (2020) 1062–1070.
[34] Y. Sun, W.Z. Xu, C. Jiang, et al., Front. Bioeng. Biotechnol. 10 (2022) 1074083.
[35] U.S. Jonnalagadda, X. Su, J.J. Kwan, Ultrason. Sonochem. 73 (2021) 105530.
[36] M. Janczarek, E. Kowalska, Catalysts 11 (2021) 978.
[37] A. Naldoni, M. Allieta, S. Santangelo, et al., J. Am Chem. Soc. 134 (2012) 7600–7603.
[38] Z. Wang, C.Y. Yang, T.Q. Lin, et al., Adv. Funct. Mater. 23 (2013) 5444–5450.
[39] H. Xu, Y.W. Hu, D. Huang, et al., ACS Sustain. Chem. Eng. 7 (2019) 5784–5791.
[40] K.H. Ye, K.S. Li, Y.R. Lu, et al., Trends Anal. Chem. 116 (2019) 102–108.
[41] L.H. Bian, N. Wang, K. Tuersong, et al., Colloids Surf. B: BioInterfaces 229 (2023) 113427.
[42] S.J. Guan, Y.L. Cheng, L. Hao, et al., Sci. Rep. 13 (2023) 14105.
[43] W. Choi, A. Termin, M.R. Hoffmann, J. Phys. Chem. 98 (1994) 13669–13679.
[44] Y.T. Lin, C.H. Weng, Y.H. Lin, et al., Sep. Purif. Technol. 116 (2013) 114–123.
[45] C.C. Yang, C.X. Wang, C.Y. Kuan, et al., Antioxidants 9 (2020) 880.
[46] Y. Xue, L. Zhang, F.W. Liu, et al., J. Control. Release 363 (2023) 657–669.
[47] M.Z. Xie, L.Q. Jing, J. Zhou, et al., J. Hazard. Mater. 176 (2010) 139–145.
[48] M. Yang, W.Z. Ren, H.J. Cui, et al., ACS Appl. Mater. Interfaces 15 (2023) 20800–20810.
[49] S. Bai, N.L. Yang, X.W. Wang, et al., ACS Nano 14 (2020) 15119–15130.
[50] Q.Q. Chen, M. Zhang, H. Huang, et al., Adv. Sci. 10 (2023) 2206244.
[51] W.J. Sun, X.J. Dong, P.P. Huang, et al., RSC Adv. 11 (2021) 36920–36927.
[52] Y.J. Liu, J.M. Szeifert, J.M. Feckl, et al., ACS Nano 4 (2010) 5373–5381.
[53] M. Ahamed, M.A.M. Khan, M.J. Akhtar, et al., Sci. Rep. 7 (2017) 17662.
[54] B.J. Geng, X. Yang, P. Li, et al., ACS Appl. Mater. Interfaces 13 (2021) 45325–45334.
[55] A.A. Lopera, A.M.A. Velásquez, L.C. Clementino, et al., J. Photochem. Photobiol. B 183 (2018) 64–74.
[56] R. Imani, R. Dillert, D.W. Bahnemann, et al., Small 13 (2017) 1700349.
[57] Y. Gong, D.X. Fu, M.M. Fan, et al., ACS Appl. Mater. Interfaces 16 (2024) 4793–4802.
[58] L.J. Chen, J.F. Zhu, J. Song, et al., Int. J. Biol. Macromol. 259 (2024) 129405.
[59] T. Dai, W.M. He, S.S. Tu, et al., Bioact. Mater. 17 (2022) 18–28.
[60] S.C. Xu, Z.Y. Qian, N.Y. Zhao, W.Z. Yuan, J. Colloid Interface Sci. 654 (2024) 1431–1446.
[61] Z.L. Li, Z.Q. Li, C.L. Zuo, X.S. Fang, Adv. Mater. 34 (2022) 2109083.
[62] A. Kumar, M. Khan, J.H. He, I.M.C. Lo, Water Res. 170 (2020) 115356.
[63] H.J. Li, Y. Zhou, W.G. Tu, et al., Adv. Funct. Mater. 25 (2015) 998–1013.
[64] B.J. Geng, S. Xu, P. Li, et al., Small 18 (2021) 2103528.
[65] J. Cao, Y. Sun, C. Zhang, et al., Acta Biomater. 129 (2021) 269–279.
[66] M.T. He, H.L. Yu, Y.M. Zhao, et al., Small 19 (2023) 2300244.
[67] Y.M. Zhao, J.H. Liu, M.T. He, et al., ACS Nano 16 (2022) 12118–12133.
[68] G.Q. Yang, Y. Liu, J.J. Chen, et al., Acc. Mater. Res. 3 (2022) 1232–1247.
[69] X.L. Zhu, S.M. Zhang, Y. Cao, et al., Chin. Chem. Lett. 34 (2023) 1001–8417.
[70] T.T. Zhu, M.Y. Jiang, M.R. Zhang, et al., Bioact. Mater. 9 (2022) 446–460.
[71] S.Y. Chen, Y.C. Lv, Y. Wang, et al., ACS Biomater. Sci. Eng. 9 (2023) 773–783.
[72] K. Polyak, I. Haviv, I.G. Campbell, Trends Genet. 5 (2009) 30–38.
[73] M. Deng, R. Guo, S. Zang, et al., ACS Appl. Mater. Interfaces 13 (2021) 18033–18046.
[74] S. Peng, F. Xiao, M. Chen, H. Gao, Adv. Sci. 9 (2022) e2103836.
[75] X. Tan, J.Z. Huang, Y.Q. Wang, et al., Angew. Chem. Int. Ed. 60 (2021) 14051–14059.
[76] G. Asantewaa, I.S. Harris, Curr. Opin. Biotechnol. 68 (2021) 292–299.
[77] Y. Liu, Y. Tian, Y.F. Tian, et al., Adv. Mater. 27 (2015) 7156–7160.
[78] Y. Gao, Z.B. Yin, Q. Ji, et al., J. Mater. Chem. B. 9 (2021) 314–321.
[79] Z.K. Li, Y.C. Pan, S.Y. Du, et al., Acta Pharm. Sin. B 12 (2022) 4224–4234.
[80] B. Arneth, Tumor Microenviron. Med. 56 (2020) 15.
[81] X.D Xue, H.J. Qu, Y.P. Li, Exploration 2 (2022) 20210134.
[82] Z.L. Sun, Y.L. Hou, BMEMat 1 (2023) e12012.
[83] L. Tu, Z.H. Liao, Z. Luo, et al., Exploration 1 (2021) 20210023.
[84] G.B. Yang, S.Z.F. Phua, W.Q. Lim, et al., Adv. Mater. 31 (2019) e1901513.
[85] Q.Y. Li, B. Lin, Y.Z. Li, N. Lu, Int. J. Nanomed. 16 (2021) 3875–3887.
[86] N. Tao, H.H. Li, L. Deng, et al., ACS Nano 16 (2021) 485–501.
[87] X. Guan, H.H. Yin, X.H. Xu, et al., Adv. Funct. Mater. 30 (2020) 2000326.
[88] W. Um, E.K.P. Kumar, Y. Song, et al., Carbohydr. Polym. 273 (2021) 118488.
[89] X. Wang, X. Zhong, L. Bai, et al., J. Am Chem. Soc. 142 (2020) 6527–6537.
[90] J.C. Shen, J. Karges, K. Xiong, et al., Biomaterials 275 (2021) 120979.
[91] Y. He, J.Y. Wan, Y. Yang, et al., Adv. Healthc. Mater. 8 (2019) 1801254.
[92] F. Gao, G. He, H. Yin, et al., Nanoscale 11 (2019) 2374–2384.
[93] W.X. Du, W.J. Chen, J. Wang, et al., BioMater. Adv. 136 (2022) 212794.
[94] Q. Feng, X. Yang, Y. Hao, et al., ACS Appl. Mater. Interfaces 11 (2019) 32729–32738.
[95] H.J. Zhang, F. Cao, L. Zhu, et al., ChemNanoMat 6 (2020) 984–995.
[96] S. Liang, X.R. Deng, G.Y. Xu, et al., Adv. Funct. Mater. 30 (2020) 1908598.
[97] X.X. Lu, K. Qiao, F. Shaik, et al., Nano Res. 16 (2023) 9730–9742.
[98] X.N. Lin, R. Huang, Y.L. Huang, et al., Int. J. Nanomed. 16 (2021) 1889–1899.
[99] X. Wei, Z.Y. Feng, J.B. Huang, et al., ACS Appl. Mater. Interfaces 13 (2021) 32810–32822.
[100] M.F. Wang, Z.Y. Hou, S.N. Liu, et al., Small 17 (2021) 2005728.
[101] C. Tang, H.S. Li, M. Sha, et al., Chem. Eng. J. 475 (2023) 146054.
[102] Y. Cao, T.T. Wu, W.H. Dai, et al., Chem. Mater. 31 (2019) 9105–9114.
[103] L.H. Cai, C.L. Hu, S.N. Liu, et al., Bioconjug. Chem. 32 (2021) 661–666.
[104] C.H. Kim, D.G. You, P.K. E.K, et al., Theranostics 12 (2022) 7465–7475.
[105] J. Lee, J.H. Kim, D.G. You, et al., Adv. Healthc. Mater. 9 (2020) e2000877.
[106] P. Zhao, H. Li, W. Bu, Angew. Chem. Int. Ed. 62 (2023) e202210415.
[107] S.T. Zuo, Y. Zhang, Z.Y. Wang, J. Wang, Int. J. Nanomed. 17 (2022) 989–1002.
[108] J.Y. Zhu, A. Ouyang, Z.L. Shen, et al., Chin. Chem. Lett. 33 (2022) 1907–1912.
[109] C.Y. Jia, Y.X. Guo, F.G. Wu, Small 18 (2021) 2103868.
[110] C.Y. Cao, X.R. Wang, N. Yang, et al., Chem. Sci. 13 (2022) 863–889.
[111] M. Zhang, D. Yang, C. Dong, et al., ACS Nano 16 (2022) 9938–9952.
[112] D.R. Hu, M. Pan, Y. Yang, et al., Adv. Funct. Mater. 31 (2021) 2104473.
[113] A.M. Smith, M.C. Mancini, S.M. Nie, Nat. Nanotechnol. 4 (2009) 710–711.
[114] Z.F. Wang, M. Wang, Y.R. Qian, et al., Chin. Chem. Lett. 34 (2023) 107853.
[115] D. Li, S.Q. Liu, Y. Ma, et al., Small Methods 7 (2023) 2300204.
[116] X.P. Duan, C. Chan, W.B. Lin, Angew. Chem. Int. Ed. 58 (2018) 670–680.
[117] E. Bockamp, S. Rosigkeit, D. Siegl, D. Schuppan, Cells 9 (2020) 2102.
[118] N. Ding, X.L. Liu, A.X. Meng, et al., Chin. Chem. Lett. 34 (2023) 107745.
[119] X.M. Zhao, L.Y. Zeng, N. Hosmane, et al., Chin. Chem. Lett. 30 (2019) 87–89.
[120] P.Y. Wang, H.R. Lin, C.H. Li, G. Liu, Chin. Chem. Lett. 34 (2023) 108068.
[121] L.Q. Zhou, X.L. Wu, S.Y. Huang, et al., Radiology 294 (2020) 19–28.
[122] G. Gunabushanam, L.M. Scoutt, Tech. Vasc. Interv. Radiol. 24 (2021) 100766.
[123] K. Christensen-Jeffries, O. Couture, P.A. Dayton, et al., Ultrasound Med. Biol. 46 (2020) 865–891.
[124] Q. Feng, Y. Li, X. Yang, et al., J. Control. Release 275 (2018) 192–200.
[125] V. Russo, L. Lovato, G. Ligabue, Radiol. Med. 125 (2020) 1040–1055.
[126] R.M. Mann, N. Cho, L. Moy, Radiology 292 (2019) 520–536.
[127] K.W. Xu, L.F. Jin, L. Xu, et al., J. Nanobiotechnol. 20 (2022) 315.
[128] F.M. Muller, J. Maebe, C. Vanhove, S. Vandenberghe, Med. Phys. 50 (2023) 5643–5656.
[129] L.C. Wang, A.Q. Mei, N. Li, et al., Chin. Chem. Lett. 35 (2024) 108974.
[130] A.B.E. Attia, G. Balasundaram, M. Moothanchery, et al., Photoacoustics 16 (2019) 100144.
[131] M.H.Y. Cheng, Y.L. Mo, G. Zheng, Adv. Healthc. Mater. 10 (2020) 2001549.